# Collisional Decay of a Strongly Driven Bose-Einstein Condensate

N. Katz, E. Rowen, R. Ozeri,* and N. Davidson

*Department of Physics of Complex Systems, Weizmann Institute of Science, Rehovot 76100, Israel*

(Received 5 May 2005; published 23 November 2005)

We study the collisional decay of a strongly driven Bose-Einstein condensate oscillating between two momentum modes. The resulting products of the decay are found to strongly deviate from the usual *s*-wave halo. Using a stochastically seeded classical field method we simulate the collisional manifold. These results are also explained by a model of colliding Bloch states.

DOI: 10.1103/PhysRevLett.95.220403 PACS numbers: 03.75.Kk, 03.75.Lm, 32.80.−t

The decay of many-body states coupled to a quasicontinuum of collisional products is a topic of great experimental and theoretical interest [1,2]. By strongly modulating the system this decay can be dramatically modified by splitting the spectrum [as in the well-known Mollow splitting [3]] and coupling to different spectral regions of the quasicontinuum [4]. Experimental Bose-Einstein condensation (BEC) allows us to investigate this decay in detail by use of highly controlled optical lattice potentials. Both the coherent evolution of the condensate in the lattice and the nature of the quasicontinuum can be manipulated and quantified [5].

The finite lifetime of perturbative bulk excitations in BEC, namely, Beliaev and Landau damping, has been extensively studied [6–9] and is rather well understood. These studies were extended recently to the ground state of a BEC in an optical lattice, and weak excitations over such a state, using band theory formulation [10–12].

Coherent Rabi oscillations of the condensate between two (or more) macroscopically populated momentum states can be driven by a strong moving optical lattice potential. These oscillations are described as beating between Bloch states belonging to different bands of the lattice [13,14]. Because of interaction nonlinearity, a superposition of two such beating Bloch states no longer solves the time-dependent Schrödinger equation, and thus the expected spectra and dynamics are richer than for a single Bloch state [15]. The decay of these excited states cannot be described by mean-field theory nor as an interaction between perturbative Bogoliubov quasiparticles [16] as in the Beliaev formalism.

In this Letter we study the collisional decay of such a strongly driven BEC undergoing coherent Rabi oscillations between momentum states by a resonant two-photon Bragg process [17]. We measure a clear deviation of the collisional products from the *s*-wave halo observed for collisions of a weak excitation with the BEC [1]. Using a stochastically seeded classical field Gross-Pitaevkii equation (GPE) simulation [18], we observe similar decay dynamics. These results are then explained by a model which includes collisions between Bloch states of the optical lattice as a perturbation.

As in [19], our nearly pure (∼95%) BEC of $N = 1.6(\pm 0.5) \times 10^5$ $^{87}$Rb atoms in the $|F, m_f\rangle = |2, 2\rangle$ ground state is formed in a magnetic trap with radial and axial trapping frequencies of $\omega_r = 2\pi \times 226$ Hz and $\omega_z = 2\pi \times 26.5$ Hz, respectively, leading to a healing length $\xi = 0.23$ $\mu$m. The condensate is driven by a pair of strong Bragg beams counterpropagating along the axial direction $\hat{z}$, with wave numbers $k_{d1} = -k_L$, and $k_{d2} = k_L$, with $k_L = 2\pi/780$ nm. The laser frequency is red detuned 44 GHz from the $^{87}$Rb $D_2$ transition in order to avoid spontaneous emission. The depth of the resulting optical lattice potential is characterized by the two-photon Rabi frequency $\Omega_d$. By tuning the frequency difference between the beams, we can control the velocity at which the optical lattice potential moves through the condensate and the subsequent energy of the created excitations. For perturbative excitations the resonance is found to be shifted by the mean-field interaction [2]. However, for strong excitations this shift averages to zero [14] and hence the frequency difference between the beams (in the laboratory frame) is set to $\delta_d = 2\pi \times 15$ kHz, the free-particle resonance. This leads to Rabi-like oscillations between the momentum states $k = 0$ and $k = 2k_L$.

The oscillation in the momentum of the atoms is apparent in Fig. 1, where we plot the measured average momentum per particle in the $\hat{z}$ direction as a function of time, extracted from time-of-flight images. The oscillation frequency, as obtained by a decaying sinusoidal fit, is $\Omega_d/2\pi = 8.6$ kHz.

In the strongly driven condensate, both finite-size broadening and inhomogeneous density broadening are greatly suppressed [14]. Therefore, the decay of the oscillations is mostly due to the collisions between atoms in momentum modes 0 and $2\hbar k_L$. The products of such a collision have an average momentum of $\hbar k_L$, and do not, in general, oscillate any more in momentum space. For a Bogoliubov excitation, which is a weak excitation of momentum $2\hbar k_L$ over a large condensate of zero momentum, the collisional products are known to be located on a shell in momentum space, known as the *s*-wave halo. This shell is the surface in momentum space, conserving both energy and momentum for the collision. Because of the Bogoliubov disper-

 

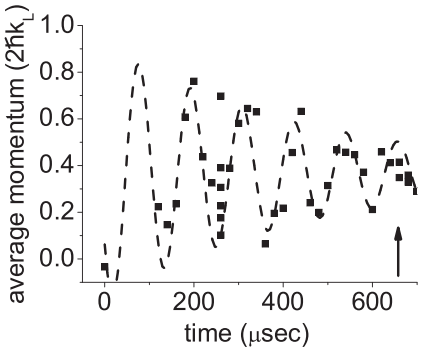


FIG. 1. Average momentum per particle contained in the atomic cloud as a function of time (in units of $2\hbar k_L$, in the laboratory reference frame). Oscillations are due to a strong moving optical lattice which is suddenly switched on, leading to Rabi oscillations between momentum wave packets. The decay in the oscillations (fit by the dashed line) is mainly due to collisions which deplete the condensate. The arrow marks the point at which Fig. 2(a) (and the subsequent theoretical figures) are taken.

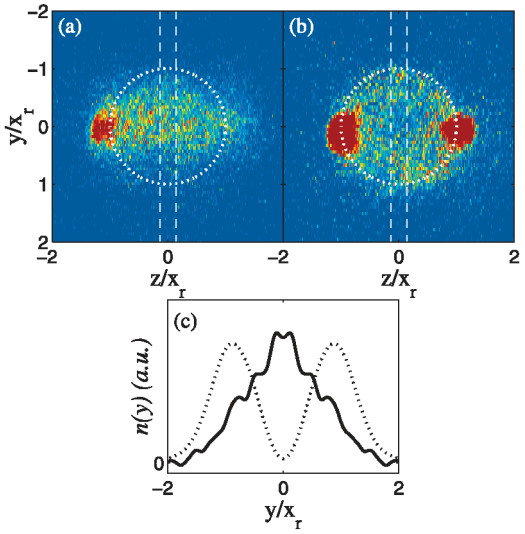


FIG. 2 (color). (a), (b) Absorption images after $t_{\rm tof} = 38$ ms time of flight following a resonant dressing pulse. (a) Strong pulse $\Omega_d/2\pi = 8.6$ kHz, pulse width $t = 660\ \mu$s. (b) Weak pulse $\Omega_d/2\pi < 2$ kHz, pulse width $t = 370\ \mu$s. Dotted circles represent the predicted $s$-wave shell. $x_r = \hbar k_L/M \times t_{\rm tof}$ is the ballistic expansion distance of an atom with wave number $k_L$ (in lattice frame of reference). The collisional manifold for the strong pulse is clearly shifted inwards as compared to that of the weak pulse, which agrees with the expected $s$-wave shell. (c) The density distribution along the $y$ axis obtained by computerized tomography [20] of the data in (a), (b) averaged over a slice marked by the vertical dashed lines. The solid line is for the strongly driven BEC of (a), and the dotted line is for the weakly excited BEC (b). The collisional products of the strongly driven BEC are clearly driven towards the center, while those of the weakly driven BEC are concentrated on the $s$-wave sphere ($y = x_r$).

sion relation, which is quadratic for $2k_L\xi > 1$, this shell is nearly spherical.

In our experiment, however, the condensate is *strongly* driven at large momentum $2k_L\xi = 3.9$, and collisions occur within the lattice potential. Consequently, the Bogoliubov description is no longer adequate. This is clearly visible in Fig. 2(a), which shows an absorption image obtained after a resonant dressing pulse lasting $t = 660\ \mu$s. Upon comparison with the $s$-wave sphere obtained when two condensates collide [Fig. 2(b)], one sees a clear shift of the collided atoms towards the center of the sphere. To quantify this difference we employ computerized tomography to extract the radial dependence of the density from the column density available in the absorption image [20]. In Fig. 2(c) we plot the radial distribution of atoms over a small slice in $\hat{z}$. This inward shift of collided atoms is robust and is clearly observed for different values of $\Omega_d$ and $t$.

We qualitatively simulate this collisional decay using the stochastically seeded classical field method, in 2D, as it was developed recently for colliding BECs [18]. In this method the initial seed of fluctuating random amplitudes of the bosonic field is added to the ground state of the condensate in the harmonic trap. Then the moving lattice potential is switched on suddenly (as in the experiment). Matter wave mixing between the condensate momentum wave packets and the seeded quasicontinuum drives the collisional decay of the oscillations, without any need for further gross numerical intervention [21]. Figure 3(a) shows the resulting momentum distributions for collisions occurring within the lattice, and Fig. 3(b) shows the collisional manifold when only a weak lattice is present. We note that the overall agreement between the simulation and experiment takes into account many possible systematic effects such as the harmonic confinement in the radial dimension and finite time of the Bragg pulse. We also see that the essential physics is qualitatively captured here, even though the simulation is not in 3D. The correlations between counterpropagating momentum wave packets, clearly visible in the simulation, are not visible in the experiment due to the fact that the experimental absorption images integrate over an additional dimension, making this signal difficult to observe. The mean-field broadening of the experimental time-of-flight images also leads to some additional smearing.

To obtain an intuitive model that still captures the essence of these phenomena, we neglect inhomogeneous and finite-size effects and choose our frame of reference as moving with the optical lattice of the Bragg lattice beams at velocity $v = -\hbar k_L/M$ along $\hat{z}$. Our system is then described by the many-body time-independent Hamiltonian

$$H = \sum_{\mathbf{k}}\left[\frac{\hbar^2 k^2}{2M}\hat{a}^\dagger_{\mathbf{k}}\hat{a}_{\mathbf{k}} + \frac{\hbar\Omega_d}{2}\left(\hat{a}^\dagger_{\mathbf{k}}\hat{a}_{\mathbf{k}-2\mathbf{k}_L} + \hat{a}^\dagger_{\mathbf{k}}\hat{a}_{\mathbf{k}+2\mathbf{k}_L}\right)\right] + \frac{g}{2V}\sum_{\mathbf{k},l,\mathbf{m}}\hat{a}^\dagger_{\mathbf{k}}\hat{a}^\dagger_{l}\hat{a}_{\mathbf{m}}\hat{a}_{\mathbf{k}+l-\mathbf{m}}, \quad (1)$$

where $\hat{a}^\dagger_{\mathbf{k}}(\hat{a}_{\mathbf{k}})$ is the creation (annihilation) operator of a

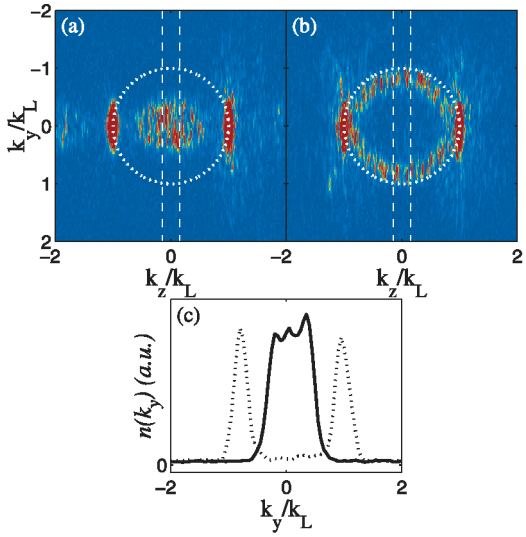


FIG. 3 (color). (a), (b) Momentum distributions generated by the classical field GPE simulation. (a) Strong pulse $\Omega_d = 8.6$ kHz, pulse width $t = 660$ $\mu$s. (b) Weak pulse $\Omega_d < 2$ kHz, pulse width $t = 370$ $\mu$s. The strong lattice leads to a clear shift of the collisional products inward as compared to the weak pulse, and deviates strongly from the $s$-wave collisional sphere. Note that the simulation also generates momentum wave packets with clear number correlations. (c) The density distribution along the $y$ axis of the simulation, averaged over a slice marked by the vertical dashed lines. The solid line is for the strongly driven BEC of (a), and the dotted line is for the weakly excited BEC (b). The inward shift, observed in the experiment [Fig. 2(c)] of the decay products is even more pronounced here.

particle with wave vector $\mathbf{k}$, and $g$ is a constant describing the $s$-wave interactions. The relative momentum in the experiment is sufficiently low to avoid higher partial wave collisional terms [22,23]. Neglecting for the moment the interaction term, Eq. (1) simplifies into a one-dimensional single particle Hamiltonian,

$$H = -\frac{\hbar^2}{2M}\frac{\partial^2}{\partial z^2} + \hbar\Omega_d \cos(2k_L z). \tag{2}$$

According to Bloch's theorem, a state $|k\rangle_w$ is only coupled to states $|k + 2pk_L\rangle_w$, where $p$ is an integer. In the moving frame of reference, the stationary BEC has momentum $\hbar k_L$ and is situated on the Brillouin zone boundary. The initial kinetic energy of the condensate is therefore in the lattice energy gap. To calculate the consequent dynamics we span the state $|k_L\rangle_w$ by the new basis of Bloch states $|n\rangle_b = \sum_p a_n[(2p+1)k_L]|(2p+1)k_L\rangle_w$, which diagonalize the Hamiltonian (2) [13], where $n$ is the Bloch band index. The lattice momentum $\hbar q = \hbar k_L$ remains unchanged and is therefore omitted. The subscript $w$ and $b$ indicate whether the quantum numbers in the ket describe the wave number of a plane wave or a Bloch band index.

In the weak lattice limit, we arrive at the two state result $|k_L\rangle_w = 1/\sqrt{2}(|1\rangle_b + |2\rangle_b)$ of a two level system undergoing Rabi oscillations with frequency $\Omega_d$. This two mode picture is still useful even for stronger lattices, since the energy separation between the lower two bands to the third band, on the edge of the Brillouin zone, is typically larger than the $\Omega_d$'s discussed here. Therefore, the higher bands are only weakly occupied by the system.

We now consider the mixing of Bloch states due to atomic interactions. In order to describe collisions, we include the interaction term in the Hamiltonian (1), which scatters two atoms from the populated states. We focus on the processes in which atoms are scattered into the quasicontinuum of unpopulated states, neglecting scattering into populated states (forward scattering) [24]. Since collisions are binary the Hilbert space is reduced to a two particle space. Hamiltonian (1) can be rewritten in the basis of the Bloch Hamiltonian (2) as

$$\begin{aligned} H = &\sum_{\nu_1,\nu_2} |\nu_1;\nu_2\rangle\langle\nu_1;\nu_2|[E_{\nu_1} + E_{\nu_2}] \\ &+ \frac{g}{2V}\sum_{\mathbf{k}_1\ldots\mathbf{k}_4,\nu_1\ldots\nu_4} \langle\nu_1|\mathbf{k}_1\rangle\langle\nu_2|\mathbf{k}_2\rangle\langle\mathbf{k}_3|\nu_3\rangle\langle\mathbf{k}_4|\nu_4\rangle \\ &\times |\nu_1,\nu_2\rangle\langle\nu_3,\nu_4|\delta_{(\mathbf{k}_1+\mathbf{k}_2)-(\mathbf{k}_3+\mathbf{k}_4)}. \end{aligned} \tag{3}$$

Here $\nu_i$ stands for all quantum numbers of a Bloch state $n_i, q_i, \mathbf{k}_{i\perp}$. $E_{\nu_i} = E_{n,q} + (\hbar k_{i\perp})^2/2M$ is the energy of the noninteracting Bloch state, where $E_{n,q}$ is an eigenvalue of the Bloch Hamiltonian (2) and $\mathbf{k}_{i\perp}$ is the part of $\mathbf{k}_i$ which is perpendicular to $\hat{z}$. The inclusion of the quantum numbers $\mathbf{k}_\perp$ is necessary since collided atoms gain momentum which is not along $\hat{z}$. We treat the collision term in Eq. (3) by use of perturbation theory. That is, we assume the system is undergoing coherent oscillations in time due to the lattice potential, and study the perturbative collisional products that are created by the interaction Hamiltonian.

The existence of two macroscopically occupied, distinct energy states implies several decay routes for the collisional term, and the subsequent energy and momentum conservation manifold are split. Specifically, splitting arises from the energy difference between the case where both colliding atoms are from the $n = 1$ band and when both are from the $n = 2$ band. Because of symmetry, interband collisions are suppressed by destructive interference. The overlap between the symmetric first band and antisymmetric second band is zero.

The prediction of our model for the momentum distribution of the collisional products is plotted in Fig. 4. The calculated column density is presented for comparison with Fig. 2.

The presence of the optical lattice is found to drive the collided atoms towards the center, as expected from the inner shell of the splitting. The amplitude of the outer shell decreases rapidly as $\Omega_d$ increases, and is experimentally unobservable for our parameters. This suppression in the amplitude of the outer collisional shell can also be understood as a quantum interference of the different collisional pathways. The antisymmetric momentum components composing the second band states lead to a small overlap with the energy-allowed collisional manifold (as observed both in the simulation and experiment). In the experimental

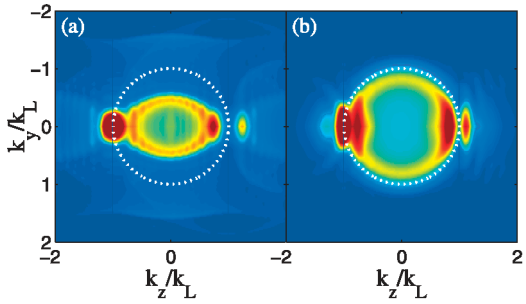


FIG. 4 (color). Column momentum distribution for the same parameters as for Figs. 2(a) and 2(b), respectively, calculated by our colliding Bloch state model [Eq. (3), only the scattered atoms are shown]. Dotted line represents the *s*-wave shell. The momentum distribution is only roughly equivalent to the spatial distributions of Fig. 2 due to interactions during expansion, although the overall shape of the collisional manifold is reproduced.

data, additional effects, such as inhomogeneous broadening and mean-field expansion effects that are neglected in this model, tend to broaden the shell of atoms, and blot out the splitting for smaller $\Omega_d$.

One intriguing prediction of the model is that the decay rate as a function of time will deviate significantly from that predicted by the Fermi golden rule. This can be explained in the time domain by the oscillatory behavior of the coherent evolution, leading to a complementary oscillation in the rate of production of collided atoms. Another important result of the model is that as we increase $\Omega_d$, the overall decay of the coherent evolution is accelerated. This is due to the large number of additional decay pathways that are switched on by the presence of a deeper lattice.

In conclusion, we measure the collisional decay of a driven condensate and show that it deviates from the usual *s*-wave sphere. This result is modeled by using the stochastically seeded classical field method applied to the Gross-Pitaevskii simulation of the experiment. The main features of the collisional decay manifold are captured by a simple model, which treats the interactions as binary collisions between single particle Bloch states. We note that the seeds for the decay of our system are the original fluctuations of the many-body ground state, while the spectra and coupling to these fluctuations are determined by the evolution of the many-body state under the strong driving. By modifying our system's spectra and thus coupling to regions of slower decay [25], it may be possible to control and even prevent decoherence.

This work was supported in part by the Israel Ministry of Science, the Israel Science Foundation, and the DIP Foundation. We thank C. Gardiner and A. Norrie for useful discussions.

*Current address: Time and Frequency Division NIST 325 Broadway Boulder, CO 80305, USA.

[1] W. Ketterle and S. Inouye, *Compte Rendus De l'academie Des Sciences*, Serie IV-Physique Astrophysique Vol. 2 (Elsevier Science, Paris, 2001), p. 339.
[2] R. Ozeri, N. Katz, J. Steinhauer, and N. Davidson, Rev. Mod. Phys. **77**, 187 (2005).
[3] B. R. Mollow, *Progress in Optics XIX*, edited by E. Wolf (North-Holland, Amsterdam, 1981), Chap. 1.
[4] M. C. Fischer, B. Gutierrez-Medina, and M. G. Raizen, Phys. Rev. Lett. **87**, 040402 (2001).
[5] I. E. Mazets, G. Kurizki, N. Katz, and N. Davidson, Phys. Rev. Lett. **94**, 190403 (2005).
[6] S. T. Beliaev, Sov. Phys. JETP **7**, 299 (1958).
[7] N. Katz, J. Steinhauer, R. Ozeri, and N. Davidson, Phys. Rev. Lett. **89**, 220401 (2002).
[8] E. Hodby, O. M. Marago, G. Hechenblaikner, and C. J. Foot, Phys. Rev. Lett. **86**, 2196 (2001).
[9] D. S. Jin, M. R. Matthews, J. R. Ensher, C. E. Wieman, and E. A. Cornell, Phys. Rev. Lett. **78**, 764 (1997).
[10] M. Kraemer, C. Menotti, L. Pitaevskii, and S. Stringari, Eur. Phys. J. D **27**, 247 (2003); D. I. Choi and Q. Niu, Phys. Rev. Lett. **82**, 2022 (1999); B. Wu and Q. Niu, Phys. Rev. A **64**, 061603(R) (2001).
[11] L. Fallani, L. De Sarlo, J. E. Lye, M. Modugno, R. Saers, C. Fort, and M. Inguscio, Phys. Rev. Lett. **93**, 140406 (2004).
[12] O. Morsch, J. H. Müller, M. Cristiani, D. Ciampini, and E. Arimondo, Phys. Rev. Lett. **87**, 140402 (2001).
[13] J. Hecker Denschlag *et al.*, J. Phys. B **35**, 3095 (2002); A. S. Mellish, G. Duffy, C. McKenzie, R. Geursen, and A. C. Wilson, Phys. Rev. A **68**, 051601(R) (2003).
[14] N. Katz, R. Ozeri, E. Rowen, E. Gershnabel, and N. Davidson, Phys. Rev. A **70**, 033615 (2004).
[15] J. Higbie and D. M. Stamper-Kurn, Phys. Rev. Lett. **88**, 090401 (2002).
[16] R. Ozeri, N. Katz, J. Steinhauer, E. Rowen, and N. Davidson, Phys. Rev. Lett. **90**, 170401 (2003).
[17] J. Stenger *et al.*, Phys. Rev. Lett. **82**, 4569 (1999).
[18] A. A. Norrie, R. J. Ballagh, and C. W. Gardiner, Phys. Rev. Lett. **94**, 040401 (2005).
[19] J. Steinhauer, R. Ozeri, N. Katz, and N. Davidson, Phys. Rev. Lett. **88**, 120407 (2002).
[20] R. Ozeri, J. Steinhauer, N. Katz, and N. Davidson, Phys. Rev. Lett. **88**, 220401 (2002).
[21] The simulation was carried out on a $2048 \times 256$ grid, with the trapping frequencies and total number of atoms as in the experiment. The ground state was found by imaginary time relaxation and the Gaussian noise seed was then added as in [18]. The dynamical evolution was calculated using the Fourier split-operator method, and applying a projector operator [18] to remove unphysical high-momentum excitations.
[22] N. R. Thomas, N. Kjaergaard, P. S. Julienne, and A. C. Wilson, Phys. Rev. Lett. **93**, 173201 (2004).
[23] Ch. Buggle, J. Léonard, W. von Klitzing, and J. T. M. Walraven, Phys. Rev. Lett. **93**, 173202 (2004).
[24] Although the weight of such processes is of order $N$ larger than the former, this approach is justified by the observation that the mean-field shift is being averaged out by the rapid oscillations [14]. Its contribution is therefore suppressed.
[25] A. G. Kofman and G. Kurizki, Phys. Rev. Lett. **87**, 270405 (2001).